

# **Fleischner Lecture Radionuclides and the Lung: Past, Present, and Future**

J. M. B. Hughes<sup>1</sup>

This, the nineteenth lecture commemorating the Austrian-born radiologist Felix G. Fleischner, was delivered in New York City, April 27, 1989. Dr. Fleischner was born in Austria 2 years before Roentgen discovered X-rays. Würzburg, where Roentgen worked, is only 250 miles from Vienna. In the 1920s, when Fleischner began his career as a radiologist, Vienna was one of the leading diagnostic radiology centers. His pioneering observations were made there between the two world wars. After emigrating to the United States in 1938, he began his second career, in Boston, MA. As director of the Department of Radiology at the Beth Israel Hospital (appointed 1942), he reflected on his early discoveries in the light of newer knowledge of anatomy, physiology, and pathology in a series of classic radiologic articles. A selected bibliography (Table 1) shows that Fleischner's early discoveries bore fruit in these classic articles in later years. He established the tradition that the radiologist must keep abreast of advances in other medical disciplines. Eight of the 19 Fleischner lectures have been given by specialists outside radiology—in pathology, physiology, anatomy, surgery, and medicine—something of which Fleischner would have approved. Not many are appointed to the staff of the Massachusetts General Hospital at the age of 73 (in an honorary capacity, admittedly), nor did Felix Fleischner's scientific output decline with his retirement; he published 22 papers after the age of 67.

*AJR* 155:455-463, September 1990

## **Early Studies with Scintillation Detectors**

Fleischner's era preceded the days of radionuclide investigation of the lung. The first person to study regional lung function by using external counting was a physician from West Germany. Born 2 years after Fleischner, H. W. Knipping was Professor of Medicine in Cologne from 1939 to 1960. An obituary by his friend Paul Sadoul (from nearby Nancy in France) stresses his creativity and enthusiasm for pulmonary research. In his pioneering experiments, human subjects inhaled methyl iodide vapor labeled with iodine-131, which was deposited in the periphery of the lung in proportion to regional ventilation and subsequently removed in proportion to local blood flow [1]. Later, Knipping and his colleagues [2] switched to a reactor-produced radioactive gas, xenon-133, with a convenient physical half-life of 5 days. This gas was relatively insoluble, suitable for studies of regional ventilation; when dissolved in saline and injected IV, measurements of pulmonary blood flow could be made also. This was Knipping's most important contribution because xenon-133 was taken up by D. V. Bates and his colleagues in Montreal [3] and J. B. West and co-workers at Hammersmith [4], and much physiological knowledge has stemmed from its use. Today xenon-133 is still the most widely used radionuclide for clinical ventilation scanning, although xenon-127, krypton-81m, and radiolabeled aerosols are tending to replace it.

Received January 31, 1990; accepted after revision April 2, 1990.

Presented at the the annual meeting of the Fleischner Society, New York, NY, April 1989.

<sup>1</sup>Department of Medicine, Royal Postgraduate Medical School, Hammersmith Hospital, London W12 0HS, England. Address reprint requests to J. M. B. Hughes.

0361-803X/90/1553-0455  
© American Roentgen Ray Society

TABLE 1: Selected Bibliography of Felix G. Fleischner

Before World War II (Austria)	After World War II (USA)
Regarding localization of free pleural effusion [in German]. <i>Wien Klin Wochenschr</i> 1926;39:642	Atypical arrangement of free pleural effusion. <i>Radiol Clin North Am</i> 1963;1:347
The visible bronchial tree: a differential diagnosis symptom in the radiologic appearance of pneumonia [in German]. <i>Fortschr Geb Rontgenstr Nuklearmed Ergänzungsband</i> 1927;36:319	The visible bronchial tree: A roentgen sign in pneumonia and other pulmonary consolidations. <i>Radiology</i> 1948;50:184-189
Regarding the presence of horizontal linear opacities in the lung field [in German]. <i>Wien Arch Innere Med</i> 1936;28:461	Linear shadows in the lung fields. <i>AJR</i> 1941;46:610

At about this time, the Medical Research Council of Great Britain had commissioned a cyclotron at Hammersmith Hospital to produce neutrons for radiotherapy. A spin-off from neutron bombardment (not originally foreseen) was the production of positron-emitting radionuclides of oxygen, nitrogen, and carbon with short physical half-lives (2.1 min for  $^{15}\text{O}$ , 10 min for  $^{13}\text{N}$ , and 20 min for  $^{11}\text{C}$ ). Consequently, 99% of the gases in the lung ( $\text{O}_2$ ,  $\text{N}_2$ , and  $\text{CO}_2$ ) could be radiolabeled and detected by external imaging. The most remarkable results were obtained with inhaled  $\text{C}^{15}\text{O}_2$  [5], as shown in Figure 1, and systematic, gravity-dependent gradients of ventilation and blood flow were clearly shown for the first time.  $\text{CO}_2$  was a particularly suitable tracer (better than Knipping's methyl iodide) because of its high solubility and diffusivity and its instantaneous entry into the lung water pool (catalyzed by carbonic anhydrase) as  $\text{H}_2^{15}\text{O}$ .

About 30 years later [6], we showed that any lipophilic substance, even a radioaerosol of the diamine molecule HMPAO (hexamethyl pentanoic-amine oxine) will be cleared with kinetics similar to those of a soluble gas such as  $\text{CO}_2$  (Fig. 2). In 1989, in contrast to 1959,  $\gamma$ -camera imaging has replaced single detectors, and computer displays (in color) show the arrival of the rapidly absorbed tracer in the kidney. In fact (Fig. 2, upper right panel) about 30% of the inhaled diamine is trapped in the epithelial and endothelial cells of the lung (by glutathione-dependent metabolic processes), and the  $\text{C}^{15}\text{O}_2$  signal is actually much clearer.

The importance of gravity was clear from the outset. Studies in most postures have shown that ventilation and blood flow are greater in the dependent part than in the nondependent part of the body. The main exception is the prone posture (ventral surface supported), where the usual gradient in the vertical direction disappears for ventilation and lung expansion but not for pulmonary blood flow [7-9]. The major contribution on the mechanisms of the ventilation gradient came from Milic-Emili and his colleagues [10] in 1966 with the famous onion-skin diagram, which relates the fractional expansion of regions to the overall expansion of the lung. The mechanism lies in the shape of the alveolar distensibility or compliance

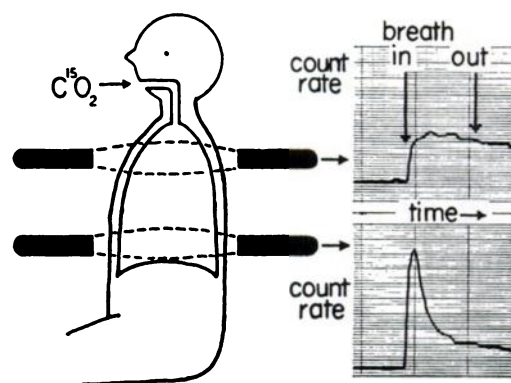


Fig. 1.—First demonstration, using radioisotopes, of a systematic gravity-linked gradient of blood flow and ventilation in lung [5]. After inhalation of air labeled with tracer quantities of  $\text{C}^{15}\text{O}_2$ , pairs of scintillation counters at different lung levels record count rate against time during breath-holding. Initial upstroke is proportional to regional ventilation and subsequent slope (clearance rate) reflects regional blood flow. Time markers are about 5 sec. Note relative increase of  $\dot{V}$  and  $\dot{Q}$  in lower zone. (Reprinted with permission from West [4].)

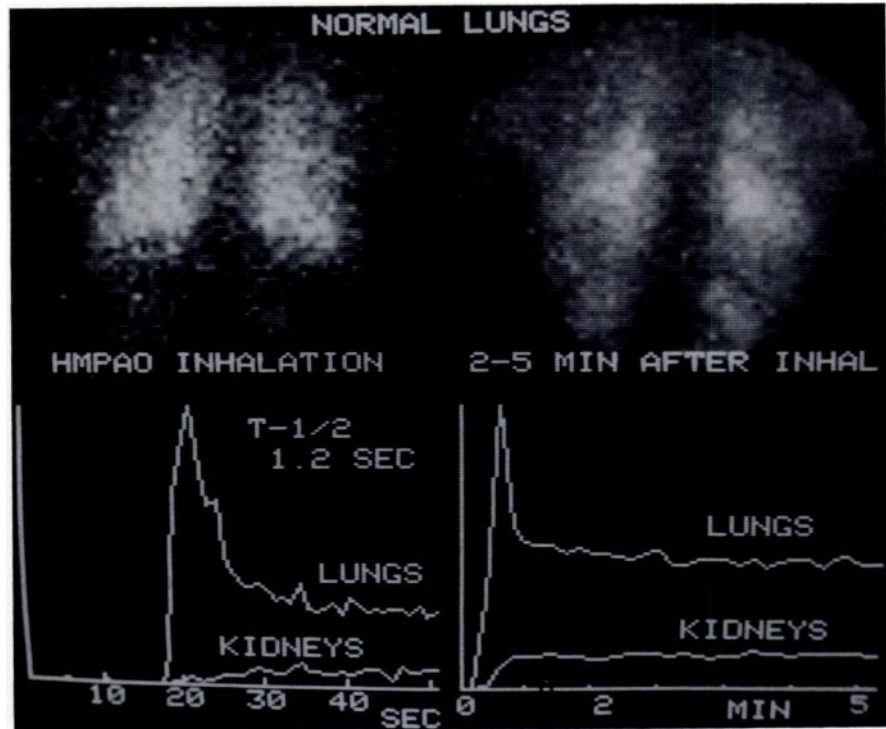
curve (lung pressure/volume relationship) whereby large alveoli are stiffer than small alveoli. The reason that dependent alveoli are smaller is that they are compressed by the weight of the lung above. The distribution of alveolar size is not the only determinant of regional ventilation, and review articles [11, 12] should be consulted for more information.

Nongravitational factors also influence blood flow, particularly the distribution of blood flow between acini within a lobule, but this is difficult to detect with the spatial resolution of radioisotope imaging systems. Vasoconstriction and reductions of lung volume can be associated with reductions in blood flow in the gravity axis (called Zone 4 [13]), and some horizontal gradients in the decubitus position are incompletely explained [7-9]. Hakim et al. [14] have described contours of isoflow radiating out from the hilum; the notion is that pulmonary vascular resistance is proportional to the vascular path length, that is, distance from the hilum. Although this is an attractive idea to explain the preferential perfusion of the proximal parts of lobules, for which there is experimental evidence [15], the distribution of blood flow on a macroscopic scale is essentially gravity dominated.

### Clinical Studies

The pioneer in use of radionuclides in pulmonary medicine was George Taplin from UCLA. He devised the beautifully simple technique of imaging the distribution of pulmonary blood flow with IV injections of aggregated albumin radiolabeled with  $^{99\text{m}}\text{Tc}$  [16]. He showed the feasibility of substituting radioaerosols for radioactive gas in the measurement of regional ventilation [17]. He explored the use of radionuclides to detect lung damage in humans [18]. All of these techniques are now widely used. Unfortunately, his premature death prevented him from delivering the 1980 Fleischner lecture.

Fig. 2.—Posterior images immediately after (left) and 2–5 min after (right) inhalation of a lipophilic aerosol (HMPAO, molecular weight 354) by a normal subject. Radioactivity is visible in kidneys below lung images. Lower panels plot rate of clearance from right lower zone and appearance in kidneys. (Reprinted with permission from Arnot et al. [6].)



### Pulmonary Embolism

Taplin's lung perfusion scan ( $\dot{Q}$  scan) has made a major contribution to clinical medicine in the diagnosis of pulmonary embolism (PE). Figure 3 shows an example of multiple segmental and sublobar loss of perfusion in the presence of normal ventilation distribution, a pattern that most would regard as diagnostic of PE. The pattern of high ventilation-perfusion ( $\dot{V}/\dot{Q}$ ) ratios in several regions is called " $\dot{V}/\dot{Q}$  mismatch" in nuclear medicine parlance. There has been considerable controversy over the sensitivity and specificity of the  $\dot{Q}$  scan in the diagnosis of PE [19]. Certain ground rules have emerged:

1. Multiple views to include right and left oblique are required.
2. A normal  $\dot{Q}$  scan excludes PE at the time of the examination but says nothing about past or future events.
3. An abnormal  $\dot{Q}$  scan may occur with any form of intrapulmonary disease, even hypoxic vasoconstriction, but clinical suspicion, a clear chest radiograph, and a negative history for pulmonary disease may tip the balance in favor of PE.
4. Nevertheless, pulmonary disease may be silent, and it is good practice to do a ventilation ( $\dot{V}$ ) scan on the basis that significant intrapulmonary disease will affect the  $\dot{V}$  and  $\dot{Q}$  scans similarly, giving "matched defects."

For efficacy assessment of radionuclide  $\dot{V}/\dot{Q}$  scans in diagnosing PE, the pulmonary angiogram is generally taken as

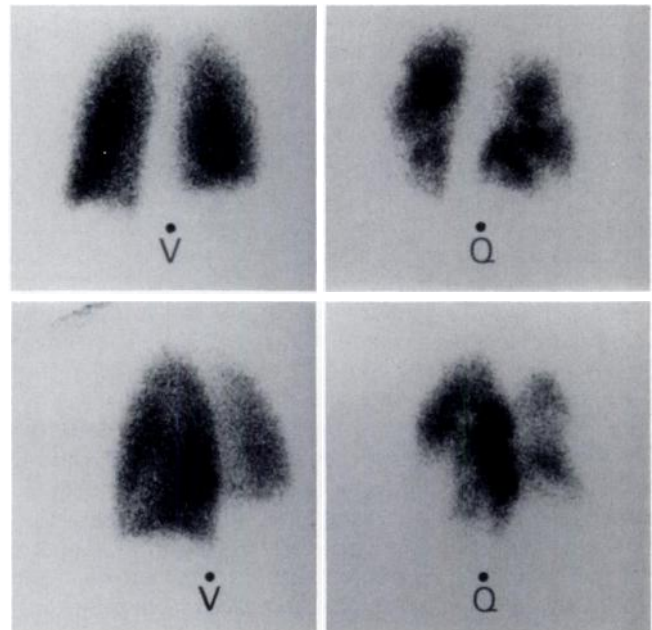


Fig. 3.—Posterior (top) and left posterior oblique (bottom) images of ventilation ( $\dot{V}$ ) (krypton-81m gas inhalation) and perfusion ( $\dot{Q}$ ) ( $^{99m}\text{Tc}$ -albumin macroaggregate injection) in a 58-year-old woman, 10 days after sigmoid colectomy. Abnormal  $\dot{Q}$  scan with normal  $\dot{V}$  scan ( $\dot{V}/\dot{Q}$  mismatch) is typical of pulmonary embolic disease.

the gold standard. Most studies have been retrospective; the first large prospective study came from McMaster University (R. D. Hull and colleagues [20]). It was an important study, not just because of the controversy it caused, but because it

TABLE 2: Analysis of 173 Patients with Suspected Pulmonary Embolism Who Had Abnormal Perfusion Scans

Group (no. of cases)	$\dot{V}/\dot{Q}$ mismatch		$\dot{V}/\dot{Q}$ match	
	I (56)	II (39)	III (51)	IV (27)
Type	Segmental	Subsegmental	Clear radiograph	Unclear radiograph
Pulmonary angiography positive (%)	87	40	40	21
Impedance plethysmography positive (%)	50	15	20	21
Probability of pulmonary embolism	High	Medium	Medium	Low
Is angiography necessary?	No	?	?	No

Note.—Data from Hull et al. [20].

focused attention on the diagnosis of deep venous thrombosis (DVT), the source of the pulmonary emboli. The case load [20] consisted of 305 consecutive patients referred with suspected PE and abnormal perfusion scans. Two hundred two patients had pulmonary angiograms (29 were technically inadequate) and, finally, only 173 patients had the necessary combination of pulmonary angiography, lower limb impedance plethysmography, and  $\dot{V}/\dot{Q}$  scanning for subsequent analysis. The results are summarized in Table 2, which shows the angiographic and impedance findings for different patterns of  $\dot{V}/\dot{Q}$  scans. For all groups, the frequency of DVT (assessed by impedance plethysmography) was low, only half as frequent as thromboembolism (assessed by angiography). This casts doubt on the sensitivity of plethysmography. Group I (one third of the analyzed cases), represents the so-called classical  $\dot{V}/\dot{Q}$  scan appearance for PE. More than 85% had abnormal angiograms; normally, pulmonary angiography is not needed in this group if the clinical picture is consistent. Group IV represents a matched  $\dot{V}/\dot{Q}$  defect associated with shadowing on radiographs, a pattern that would normally be consistent with pulmonary disease but that could, in the right setting, be pulmonary infarction. Angiograms positive for PE were uncommon (6/173 cases analyzed), but if clinical suspicion is high, screening for DVT might be undertaken.

The findings in Groups II and III are rather hard to explain. In Group II, a  $\dot{V}/\dot{Q}$  mismatch, even at a subsegmental level, suggests PE but, according to Hull et al. [20], 60% will have normal findings on angiograms. Does the fault lie with the angiogram or with the  $\dot{V}/\dot{Q}$  scan? Was the  $\dot{Q}$  scan falsely positive for PE? Would more rigorous technique with oblique views and/or single-photon emission CT (SPECT) have helped? Was the  $\dot{V}$  scan falsely normal so that the  $\dot{Q}$  defects were really matched with them, suggesting pulmonary disease? How accurate is the diagnosis of PE with pulmonary angiography? Without selective injections (not made routinely in this series), small defects may easily be missed on angiography. The interpretation of minor defects is difficult (more art than science), and radiologists often fail to agree. For example, in the PIOPED study (see below) more than 80% agreement in angiographic interpretation (for or against PE) between radiologists was seen for segmental and lobar arteries. Agreement was relatively poor for peripheral arteries. An independent panel should probably have been called in to assess the films. So the gold standard itself may be imperfect. Likewise, in Group III (matched defects with clear chest radiograph, typical of chronic obstructive pulmonary disease) the figure of 40% angiograms positive for PE seems remark-

ably high. The Hull article unfortunately does not go into detail over the angiographic criteria used, but arterial "cut-off" in the absence of intravascular filling defects caused by clot may indicate vascular destruction rather than obstruction.

The most definitive study of the diagnosis of PE is most likely the PIOPED study (Prospective Investigation of Pulmonary Embolism Diagnosis). More than 1400 patients were recruited prospectively at six institutions. In the largest subgroup evaluated, 755 pulmonary angiograms (251 positive for PE) and  $\dot{V}/\dot{Q}$  scans were analyzed. The final results have not been published, but preliminary reports show that 88% of the high probability group on  $\dot{V}/\dot{Q}$  scanning (Group I of Hull et al. [20]) had angiograms positive for PE. Only 15% of low probability  $\dot{V}/\dot{Q}$  scans (e.g., nonsegmental  $\dot{Q}$  defects,  $\dot{Q}$  defects associated with a larger opacity shown on radiographs, matching  $\dot{V}$  and  $\dot{Q}$  defects, a single subsegmental  $\dot{Q}$  defect) had angiograms positive for PE. This is more encouraging than the Hull data are [20].

For the future, we may expect to see the development of specific thrombus-seeking agents. J. P. Lavender and A. M. Peters [21, 22] have investigated P256, a monoclonal antibody directed against the fibrinogen receptor on the surface of platelets. P256 can be labeled with  $^{111}\text{In}$  and has been injected IV into postoperative patients. Clear images of thrombus are obtained after 24 hr, with regions of higher radioactivity seen in the calf and in the lungs, where they correspond to perfusion defects on the blood flow scan. Monoclonal antibodies against fibrin also have been developed [23] and used clinically to detect venous thrombus. Both these and the antiplatelet antibodies [24] can be labeled with  $^{99\text{m}}\text{Tc}$  in order to achieve better and earlier imaging. If these agents or others that are being developed are used prospectively in groups of patients who are at risk, the frequency of silent DVT and PE may be much greater than we imagined. Evidence that DVT is associated frequently with unsuspected pulmonary embolic disease already exists [25]. The use of radiolabeled monoclonal antibodies as thrombus-seeking agents should be more specific for PE (and DVT) than lung perfusion scans or pulmonary angiography.

#### Arteriovenous Shunt

The lung perfusion scan has other applications. For example, in pulmonary arteriovenous communications, the radiolabeled 20- to 40- $\mu\text{m}$  albumin microspheres, which are smaller than the shunt channels, pass through the lung and lodge in

systemic tissues in proportion to their share of the cardiac output. If corrections are made for tissue attenuation, good correlation exists between the shunt measured from lung/dose or kidney/dose ratios and that measured simultaneously by the classical 100% oxygen method [26] in patients with pulmonary arteriovenous communications. The microsphere method is simpler for patients than 15 min oxygen breathing from a Douglas bag and arterial sampling. In some patients with liver disease, the pulmonary arteriovenous communications, although larger than 30- $\mu\text{m}$  diameter, are so small that they take part, although imperfectly, in pulmonary gas exchange. Under these circumstances, the shunt with  $^{99\text{m}}\text{Tc}$ -labeled microspheres is greater than the shunt measured with oxygen [27] (another of G. V. Taplin's contributions).

### Ventilation Measured with Radioaerosols

George Taplin was one of the first to explore the possibility of measuring regional ventilation with inhaled radiolabeled aerosols [17] (one of his earliest scientific papers looked at the feasibility of administering penicillin as an aerosol). Of course aerosols are easier to administer and dispose of than radioactive gases. In normal lungs, only trivial differences between aerosol and radioactive gas distributions are discernible by external imaging, provided the particle does not exceed 1–2  $\mu\text{m}$  median diameter. On the other hand, in the presence of air-flow obstruction (Fig. 4), a discordance occurs between gas and aerosol distributions that is proportional to the severity of disease [28]. Except for aerosol deposition in the most central airways, the spotty peripheral distribution of the aerosol could be due either to airway impaction on bronchial walls, especially at bifurcations where there is increased turbulence, or to the uneven distribution of *convective* flow (radioactive gases that are transported by molecular diffusion

and by convection would be distributed more widely). I favor the second explanation, which implies that an aerosol scan magnifies any maldistribution of inspired ventilation.

This amplification factor means that radioaerosol scans are probably more sensitive than ventilation scans with radioactive gases in detecting early bronchial disease, for example, in asymptomatic smokers. Nevertheless, the clumping of aerosol particles seen in moderately severe air-flow obstruction (Fig. 4, bottom right) is a nuisance when a  $\dot{V}/\dot{Q}$  mismatch suggestive of PE (Fig. 3) is being sought. Better nebulizers providing smaller aerosol particles may be a partial solution.

### $^{99\text{m}}\text{Tc}$ -DTPA Aerosol and Lung Injury

Another pioneering step taken by Taplin was the introduction of radiolabeled aerosols of small-molecular-weight molecules, such as DTPA (molecular weight, 393) [18]. DTPA (diethylenetriamine pentacetate) is lipophobic and penetrates the tight junctions between alveolar and airway epithelium with difficulty. Nevertheless, after inhalation as a finely dispersed aerosol and dispersion throughout the lung periphery, its clearance half-time of 50–70 min is much shorter than an aerosol of albumin (MW 48,000) whose removal ( $t_{1/2}$ ) by mucociliary clearance takes 150–300 min. The lung clearance of aerosols of lipophobic molecules from the alveolar liquid layer, where they are deposited, into the pulmonary circulation is (in terms of  $t_{1/2}$ ) proportional to molecular weight [29]. Electrical charge also has an effect [29]. The original studies of Chopra et al. [18] showed that pertechnetate ( $\text{TcO}_4$ , MW 168) is cleared faster than  $^{99\text{m}}\text{Tc}$ -DTPA but that the latter is a better marker of lung injury (Fig. 5). The clearance of all these molecules is said to be *diffusion-limited*. Their clearance rates are of a completely different magnitude than those of rapidly diffusing substances such as lipophilic aerosols (HMPAO, Fig.

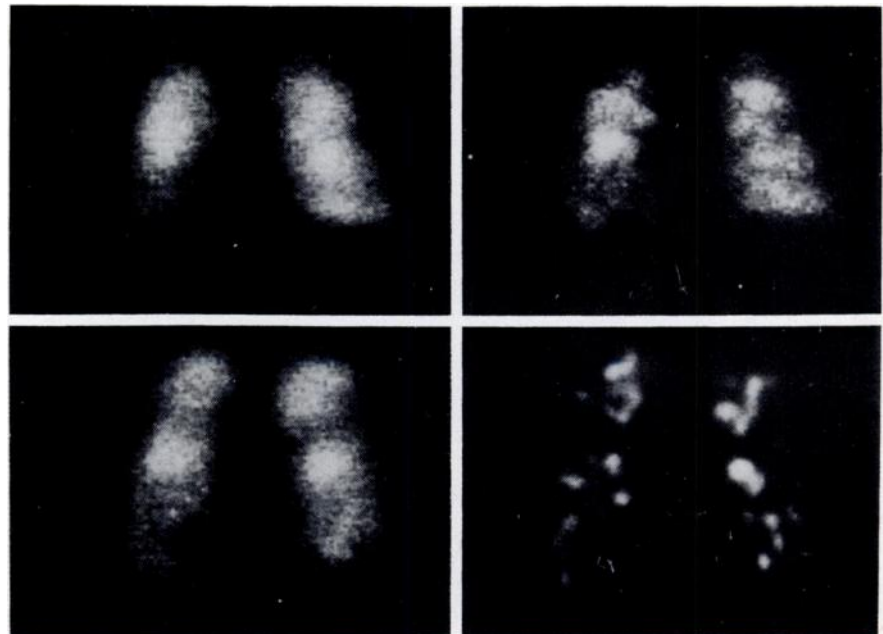


Fig. 4.—Posterior ventilation images using  $^{81\text{m}}\text{Kr}$  gas (left) and an ultrafine  $^{99\text{m}}\text{Tc}$  aerosol (0.12- $\mu\text{m}$  particle size) (right) in two patients with asthma, one with mild air-flow obstruction (top) and one with moderate obstruction (bottom). Note exaggerated inhomogeneity with aerosol compared with gas. (Reprinted with permission from Arnot et al. [28].)

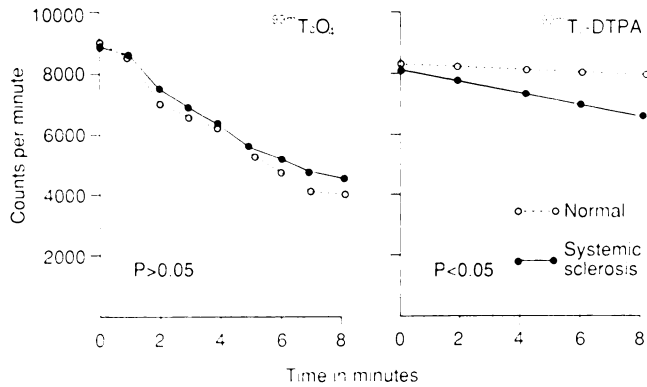


Fig. 5.—Radioactivity plotted against time over lower zones of normal subjects ( $n = 7$ ) and patients with systemic sclerosis with shadowing on radiographs and impaired lung diffusing capacity ( $n = 10$ ), after inhalation of  $^{99m}\text{TcO}_2$  (molecular weight 163) or  $^{99m}\text{Tc-DTPA}$  (molecular weight 492) aerosols. Note more rapid disappearance of  $^{99m}\text{TcO}_2$ , but better discrimination for injury with  $^{99m}\text{Tc-DTPA}$  clearance. (Reprinted with permission from Chopra et al. [18].)

2) or gases such as  $\text{C}^{15}\text{O}_2$  (Fig. 1), whose clearance is perfusion-limited.

Jones et al. [30], quite independently of Taplin's work, had been measuring the lung-to-blood clearance in anesthetized rabbits of airway instillation of a solution of  $^{51}\text{Cr-EDTA}$  (a molecule similar to DTPA) and  $^{125}\text{I-antipyrine}$  (IAP). Later, Jones and his colleagues at Northwick Park Hospital in London [31] made the remarkable observation, using Taplin's method [18], that the  $^{99m}\text{Tc-DTPA}$  aerosol clearance was twice as fast in cigarette smokers (apparently perfectly healthy) as in nonsmokers (Fig. 6). Later work from the same group [32] showed that after the person stopped smoking, the clearance returned toward normal (although it remained abnormal) 2–3 weeks later. The mechanism of the increase in  $^{99m}\text{Tc-DTPA}$  clearance in healthy smokers is still unexplained [33], but these findings were the stimulus for much research and more than 100 papers have appeared in which  $^{99m}\text{Tc-DTPA}$  clearance has been measured in many situations and clinical conditions [34]. The findings of Chopra et al. [18] of increased clearance in systemic sclerosis have been confirmed in different types of interstitial lung disease many times [35]. Adult respiratory distress syndrome [36, 37], *Pneumocystis pneumonia* [38], surfactant depletion by lung lavage [39], and a host of other conditions are associated with increased  $^{99m}\text{Tc-DTPA}$  aerosol clearance. The method is so sensitive that even a modest increase in lung volume (produced by positive end-expiratory pressure) will double the clearance rate [29]. The mechanism of this particular finding, as with smoking, has not been adequately explained. Background correction for intravascular and chest wall accumulation of  $^{99m}\text{Tc-DTPA}$  is an important refinement of the technique [40].

#### $^{113m}\text{In-Transferrin}$ and Microvascular Permeability

A more specific but less sensitive marker of lung injury is the microvascular escape of  $^{113m}\text{In-transferrin}$ , a radiolabeled plasma protein similar in size to albumin, after an IV injection.

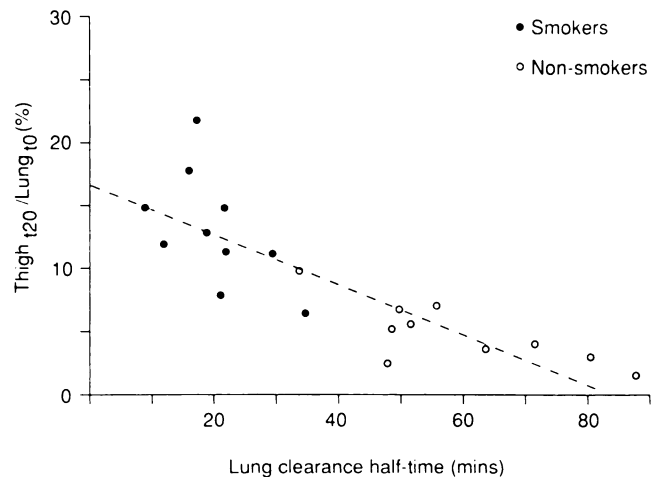


Fig. 6.—First demonstration of effect of chronic cigarette smoking on alveolar capillary permeability. Lung clearance half-time after inhalation of  $^{99m}\text{Tc-DTPA}$  aerosol (abscissa) is related to its appearance systemically (recorded by a counter on thigh) as ratio of thigh counts at 20 min to initial lung counts. Note more rapid disappearance of  $^{99m}\text{Tc-DTPA}$  from lung and its appearance systemically in smokers. (Reprinted with permission from Jones et al. [31].)

This method, introduced by Gorin et al. [41], is quite specific for microvascular injury [42] but in adult respiratory distress syndrome it is much less sensitive than  $^{99m}\text{Tc-DTPA}$  clearance [38]. Nevertheless, some interesting clinical results have been obtained that suggest that hemodynamic edema can be distinguished from permeability edema [43, 44] (Fig. 7).

One of the attractions of the  $^{99m}\text{Tc-DTPA}$  and  $^{113m}\text{In-transferrin}$  techniques is that the methods are very simple and no more than two scintillation detectors are required. Measurements can easily be made at the bedside in the intensive care setting.

#### Imaging Trapped Blood

Taplin et al. [45] and Ewan et al. [46] independently had the idea of inhaling radioactive carbon monoxide ( $^{11}\text{CO}$ ) to detect and locate trapped or stagnant blood. Taplin and coworkers were interested in finding a pool of nonflowing blood trapped beyond a pulmonary embolus. Ewan et al. wanted a method to detect the capillary hemorrhage associated with Goodpasture syndrome.  $^{11}\text{CO}$ , after inhalation, binds very firmly to hemoglobin, both intravascularly and extravascularly. Thus, in the presence of capillary hemorrhage or trapped blood, the removal of  $^{11}\text{CO}$  radioactivity from the lung counting field would be very slow, but its absorption from the inspired gas should be greater than usual. This notion proved correct [46] (Fig. 8). Again, these measurements were made with just two pairs of scintillation detectors without any imaging whatsoever!

#### Tomography (SPECT and PET)

The future prospects for radionuclide imaging are very exciting. A wide range of new radiopharmaceuticals such as

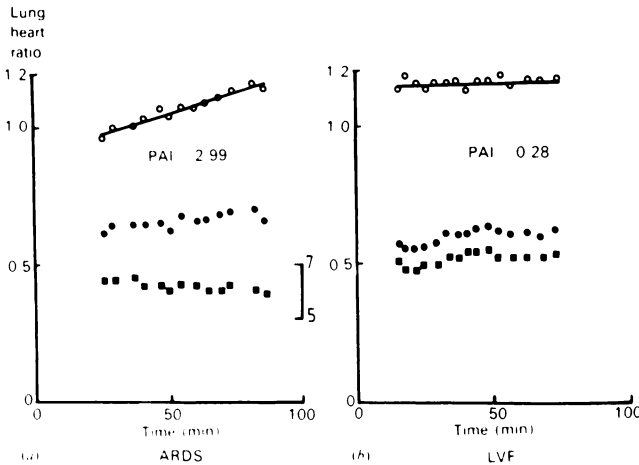


Fig. 7.—Radioactivity plotted against time in two patients with diffuse alveolar shadowing associated with the adult respiratory distress syndrome (ARDS) and left ventricular failure (LVF). Radioactivity is plotted as ratio of counts from detectors over right upper lung zone (anteriorly) and over heart (lung:heart ratio) for <sup>99m</sup>Tc-labeled red cells (■) and <sup>113m</sup>In-transferrin (●). Slope of <sup>99m</sup>Tc:<sup>113m</sup>In ratio (○) is termed protein accumulation index (PAI). A positive slope (in ARDS but not in LVF) indicates a microvascular protein leak. (Reprinted with permission from Rocker et al. [44].)

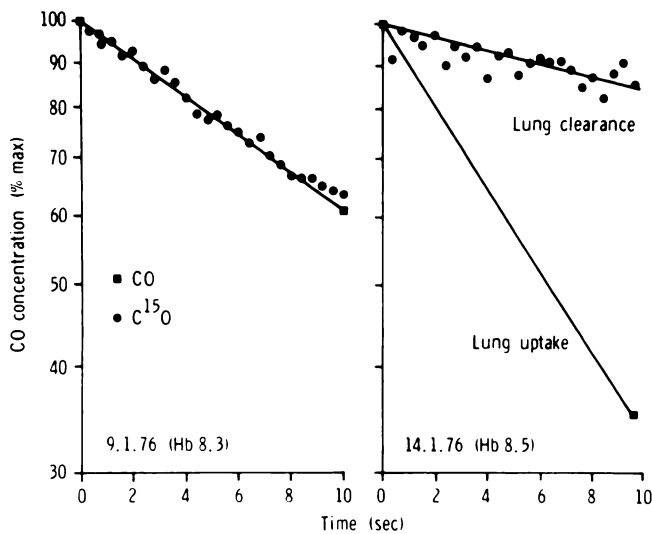


Fig. 8.—Count rate (as percentage of maximum) recorded from a scintillation detector over right upper zone anteriorly after inhalation (and subsequent breath-holding) of <sup>11</sup>C-labeled carbon monoxide in the presence (right) and absence (left) of lung hemorrhage in a patient with Goodpasture syndrome. (Reprinted with permission from Ewan et al. [46].)

metabolic markers, receptor ligands, labeled cells, and monoclonal antibodies will be imaged with planar and tomographic scanning. For the sake of brevity, I limit my discussion to the present and future contributions of tomography to pulmonary medicine. Tomography comes in two packages: SPECT for photon emitters such as <sup>99m</sup>Tc, <sup>111</sup>In, and <sup>123</sup>I with (generally) a rotating gamma camera, and PET (positron emission tomography), which in outline looks more like a CT scanner. At the moment, PET is probably the ultimate in imaging technol-

ogy. The latest generation PET scanners contain 2560 scintillation detector elements, arranged in five circular rings, from which 15 transaxial planes (0.5-cm thick) can be reconstructed.

The disadvantage of tomography is that it is slow if the maximum spatial resolution is required; up to 10 min may be required to collect statistically reliable counts for a single scan. The advantage lies in its definition of geometry in three dimensions. The accuracy of SPECT is relative because corrections for attenuation are not precise. PET uses coincidence counting (a special property of positrons), and precise quantitation of radionuclide concentrations (megabecquerels per voxel) within and between organs *in vivo* is possible for the first time. This is a major breakthrough, even though the spatial resolution, especially in the lung, is somewhat limited (0.7–1.0 cm).

For clinical purposes, the three-dimensional resolution given by SPECT may have great advantages in mapping distributions of blood flow and ventilation. For ventilation studies, the requirement for 10-min scans means that continuous inhalation of <sup>81m</sup>Kr or radiolabeled aerosols must be used, rather than <sup>133</sup>Xe. Wiener et al. [47] have shown with SPECT a decrease in ventilation of the left lower lobe in patients with cardiomegaly; the marked difference in ventilation between the right and left lungs disappeared with the patient prone (Fig. 9). Normal subjects did not show any right/left lung difference in either position. This suggests that an enlarged heart, by virtue of its ventral position in the thorax, leads to mechanical compression and hypoventilation of the left lower lobe.

The only PET application that I will mention concerns the use of <sup>18</sup>F-deoxyglucose as a metabolic tracer. Deoxyglucose after IV injection enters cells and is converted to deoxyglucose-6-phosphate (catalyzed by hexokinase). But deoxyglucose-6-phosphate, which differs from glucose-6-phosphate, is not metabolized further at any appreciable rate, and the back reaction, catalyzed by phosphatase, has a negligible rate constant. Fluorine-18, a positron emitter with a half-life of 110 min, can be substituted for hydrogen, and the rate of tissue accumulation of <sup>18</sup>F, after IV injection of <sup>18</sup>F-deoxyglucose (<sup>18</sup>FDG), represents the rate of conversion of <sup>18</sup>FDG to <sup>18</sup>FDG-6-phosphate, which is analogous to the metabolic rate for glucose (Fig. 10). <sup>18</sup>FDG has been used for some time as a metabolic marker of ischemia in the brain and the heart (energy production by anaerobic mechanisms consumes considerably more glucose per unit ATP production). Ischemia is not really a problem for lungs, which have a dual blood supply. Nevertheless, we have found other applications for <sup>18</sup>FDG. A physiologic finding was that the rate of <sup>18</sup>FDG-6-phosphate production doubled for lung tissue (also for the myocardium and chest wall tissues) after a meal, presumably reflecting the influence of insulin [48]. Second, the metabolic rate in lung neoplasms exceeded that of normal tissue several fold [49]. The most interesting application was in acute and chronic inflammation. Raised metabolic rates have been found in cryptogenic fibrosing alveolitis [50] and sarcoidosis [51] (Fig. 10) and in experimental pneumonia (*Streptococcus pneumoniae*) in rabbits (Table 3) [52]. The reason for the increased <sup>18</sup>FDG signal in inflammation is the presence of neutrophils,

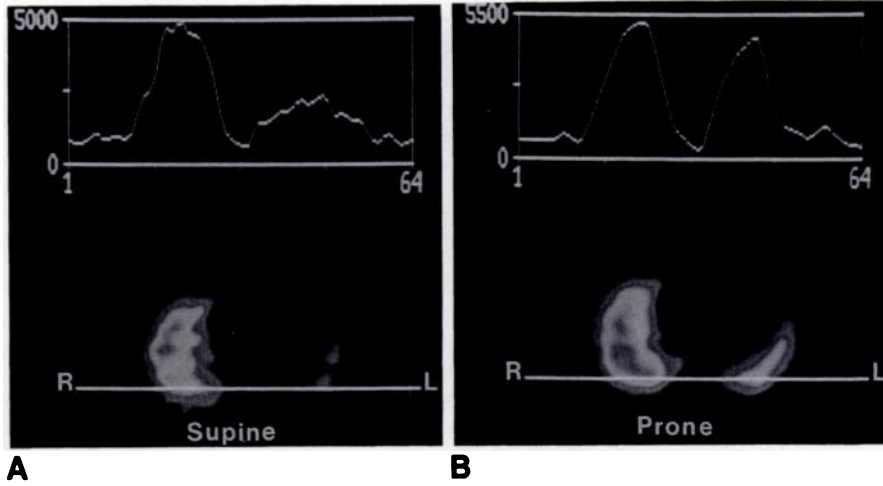


Fig. 9.—Tomographic transaxial images of ventilation by using <sup>81m</sup>Kr gas inhalation and single-photon emission CT at mid-heart level in supine (A) and prone (B) patient with cardiomegaly. Counts per pixel are plotted against distance along a horizontal axis through dorsal regions of both lungs. Note image of prone patient has been inverted. Reduced ventilation of left lower lobe in supine patient is restored when patient is prone. (Reprinted with permission from Wiener et al. [47].)

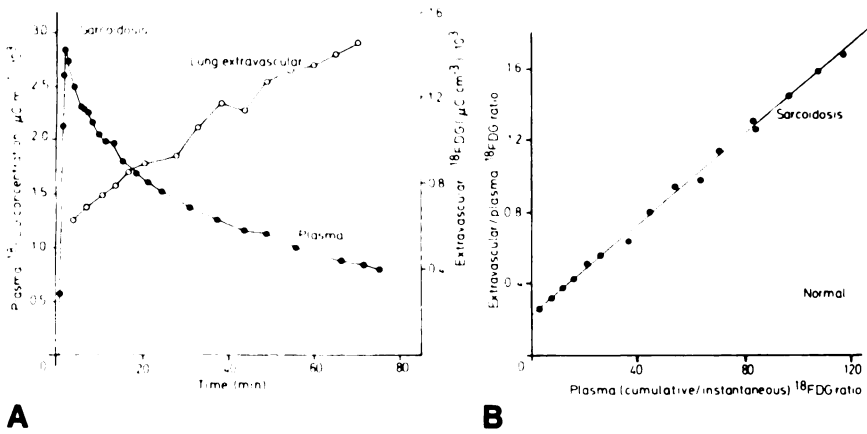


Fig. 10.—A, Plasma and extracellular lung (dorsal right lung, patient supine) <sup>18</sup>F concentrations plotted against time since IV injection of <sup>18</sup>F-deoxyglucose at time zero in a patient with sarcoidosis. Lung <sup>18</sup>F concentrations obtained by positron emission tomography (PET). B, Data derived from A, where abscissa is area under plasma curve (cumulative) up to time t divided by plasma level at time t. Slope is proportional to metabolic rate for glucose. Normal range shown. (Reprinted with permission from Hughes et al. [51].)

TABLE 3: Regional Pulmonary Glucose Metabolism Measured with Fluorine-Labeled Deoxyglucose (<sup>18</sup>FDG) and Positron Emission Tomography

Condition [ref.]	Glucose Metabolism in $\mu\text{mol } ^{18}\text{FDG g}^{-1} \text{hr}^{-1}$
Fasting [44]	1.90 (SD 0.8)
Fed [4]	5.20 (SD 1.7)
Cryptogenic fibrosing alveolitis [46]	1.14–3.75 (range)
Sarcoidosis [47]	2.26–11.39 (range)
	<i>Involved/Uninvolved Lung</i>
Carcinoma [45]	6.6 (2.7–14.6)
<i>Streptococcus pneumonia</i> [48]	7.8 (1.1–2.3)
Bleomycin injury [48]	4.5 (SD 1.1)

lymphocytes, macrophages, and other blood-derived inflammatory cells. These cells metabolize anaerobically (preferentially) because of a relative lack of oxidative enzymes. Their high metabolic rate for glucose has been demonstrated recently in experimental pneumonia by autoradiography with <sup>3</sup>H-deoxyglucose [52].

We are now turning toward imaging enzyme-substrate interactions [53] and receptor binding, following the lead given

by Farde et al. [54] (dopamine receptors in the basal ganglia) and Syrota et al. [55] (muscarinic receptors in the heart).

ACKNOWLEDGMENTS

Finally, I acknowledge how much I owe to those who introduced me to the world of nuclear medicine and regional lung function, notably J. B. West, J. Milic-Emili, J. P. Lavender, T. Jones, and C. G. Rhodes, and to those with whom I have collaborated during the past 24 years, who are too numerous to mention individually and who come from four continents and 12 different countries.

REFERENCES

- Knipping HW, Bolt W, Venrath H, Valentin H, Ludes H, Enderl P. Eine neue Methode zur Prufung der Herz und Lungenfunktion. *Dtsch Med Wochenschr* 1955;80:1146–1147
- Knipping HW, Bolt W, Valentin H, Venrath H, Enderl P. Regionale Funktionsanalyse in der Kreislaufund Lungen Klinik mit Hilfe der Isotopenthorakographie und der selektiven Angiographie der Lungengefass. *Munch Med Woch* 1957;99:1–3
- Ball WC, Stewart PB, Newsham LGS, Bates DV. Regional pulmonary function studied with xenon<sup>133</sup>. *J Clin Invest* 1962;41:519–531
- West JB. Distribution of gas and blood in the normal lungs. *Br Med Bull* 1963;19:53–58
- West JB, Dollery CT. Distribution of blood flow and ventilation-perfusion

- ratio in the lung measured with radioactive CO<sub>2</sub>. *J Appl Physiol* **1960**;15:405-410
6. Arnot RN, Takagi H, Hughes JMB, Royston D, Peters AM, Lavender JP. Alveolar clearance of aerosolized <sup>99m</sup>Tc-HMPAO. *Clin Sci* **1988**;74:60P
  7. Amis TC, Jones HA, Hughes JMB. Effect of posture on inter-regional distribution of pulmonary ventilation in man. *Respir Physiol* **1984**;56:145-167
  8. Amis TC, Jones HA, Hughes JMB. Effect of posture on inter-regional distribution of pulmonary perfusion and VA/Q ratios in man. *Respir Physiol* **1984**;56:169-182
  9. Orphanidou D, Hughes JMB, Meyers MJ, Al-Suhali AR, Henderson B. Tomography of regional ventilation and perfusion using Krypton-81m in normal subjects and asthmatic patients. *Thorax* **1986**;41:542-551
  10. Milic-Emilij J, Henderson JAM, Dolovich MB, Trop D, Kaneko K. Regional distribution of inspired gas in the lung. *J Appl Physiol* **1966**;21:749-759
  11. Engel LA. Dynamic distribution of gas flow. In: Macklem PT, Mead J, eds. *Handbook of physiology: the respiratory system*, vol. 3. Baltimore: American Physiological Society, **1986**:575-593
  12. Hughes JMB, Amis TC. Regional ventilation distribution. In: Engel LA, Paiva M, eds. *Gas mixing and distribution in the lung*. New York: Marcel Dekker, **1985**:177-220
  13. Hughes JMB, Glazier JB, Maloney JE, West JB. Effect of lung volume on the distribution of pulmonary blood flow in man. *Respir Physiol* **1968**;4:58-72
  14. Hakim TS, Lisbona R, Dean GW. Gravity-independent inequality in pulmonary blood flow in humans. *J Appl Physiol* **1987**;63:1114-1121
  15. Wagner P, McRae J, Read J. Stratified distribution of blood flow in secondary lobule of rat lung. *J Appl Physiol* **1967**;22:1115-1123
  16. Taplin GV, Johnson DE, Dore EK, Kaplan S. Lung photoscans with macroaggregates of human serum radioalbumin. *Health Phys* **1964**;10:1219-1227
  17. Taplin GV, Poe ND, Greenberg A. Lung scanning following radioaerosol inhalation. *J Nucl Med* **1966**;7:77-87
  18. Chopra SK, Taplin GV, Tashkin DP, Elam D. Lung clearance of soluble aerosols of different molecular weights in systemic sclerosis. *Thorax* **1979**;34:63-67
  19. Wellman HN. Pulmonary thromboembolism: current status report on the role of nuclear medicine. *Semin Nucl Med* **1986**;16:236-274
  20. Hull RD, Hirsh J, Carter CJ, et al. Diagnostic value of ventilation-perfusion lung scanning in patients with suspected pulmonary embolism. *Chest* **1985**;88:819-828
  21. Peters AM, Lavender JP, Needham SG, et al. Imaging thrombus with radiolabelled monoclonal antibody to platelets. *Br Med J* **1986**;293:1525-1527
  22. Stuttle AWJ, Klosok J, Peters AM, Lavender JP. Sequential imaging of post operative thrombus using In-111 labeled platelet specific monoclonal antibody. *Br J Radiol* **1989**;62:963-969
  23. Alavi A, Gupta M, Berger H, Palevsky H, Jatlow A, Kelly M. Detection of venous thrombus with In-111 labeled antifibrin 59D8 antibody imaging. *J Nucl Med* **1988**;29:825A
  24. Som PE, Oster ZH, Zamora PO, et al. Radio immune imaging of experimental thrombi in dogs using technetium-99m labeled monoclonal antibody fragments reacting with human platelets. *J Nucl Med* **1986**;27:1315-1320
  25. Moser KM, Lemoine JR. Is embolic risk conditioned by location of deep venous thrombosis? *Ann Intern Med* **1981**;94:439-444
  26. Chilvers ER, Peters AM, George P, Hughes JMB, Allison DJ. Quantification of right to left shunt through pulmonary arteriovenous malformations using Tc-99m microspheres. *Clin Radiol* **1988**;39:611-614
  27. Genovesi MG, Tierney DF, Taplin GV, Eisenberg H. An intravenous method to evaluate hypoxaemia caused by abnormal alveolar vessels: limitation of conventional techniques. *Am Rev Respir Dis* **1976**;114:59-65
  28. Arnot RN, Burch WM, Orphanidou DG, Gwilliam ME, Aber VR, Hughes JMB. Distributions of an ultra-fine <sup>99m</sup>Tc aerosol and <sup>81</sup>Kr<sup>m</sup> gas in human lungs compared using gamma camera. *Clin Phys Physiol Meas* **1986**;7:345-359
  29. Barrowcliffe MP, Zanell GD, Jones JG. Pulmonary clearance of radiotracers after positive and expiratory pressure on acute lung injury. *J Appl Physiol* **1989**;66:288-294
  30. Jones JG, Berry M, Hulands GH, Crawley JCW. Time course and degree of change in alveolar capillary membrane permeability induced by aspiration of hydrochloric acid and hypotonic saline. *Am Rev Respir Dis* **1978**;118:1007-1013
  31. Jones JG, Minty BD, Lawler P, Hulands G, Crawley JCW, Veall N. Increased alveolar permeability in cigarette smokers. *Lancet* **1980**;1:66-68
  32. Minty BD, Jordan C, Jones JG. Rapid improvement in abnormal permeability after stopping smoking. *Br Med J* **1981**;282:1184-1186
  33. Nolop KB, Maxwell DL, Fleming JS, Braude S, Hughes JMB, Royston D. A comparison of <sup>99m</sup>Tc-DTPA and <sup>113m</sup>In-DTPA aerosol clearances in humans. *Am Rev Respir Dis* **1987**;136:1112-1116
  34. Barrowcliffe MP, Jones JG. Solute permeability of the alveolar-capillary barrier. *Thorax* **1987**;42:1-10
  35. Rinderknecht J, Shapiro L, Krauthammer M, et al. Accelerated clearance of small solutes from the lungs in interstitial disease. *Am Rev Respir Dis* **1980**;121:105-117
  36. Evander E, Wollmer P, Jonson B, Lachmann B. Pulmonary clearance of inhaled <sup>99m</sup>Tc-DTPA: effects of surfactant depletion by lung lavage. *J Appl Physiol* **1987**;62:1611-1614
  37. Mason GR, Effros RM, Uszler JM, Mena I. Small solute clearances from the lungs of patients with cardiogenic and non-cardiogenic pulmonary edema. *Chest* **1985**;88:327-334
  38. Braude S, Nolop KB, Hughes JMB, Barnes PJ, Royston D. Comparison of lung vascular and epithelial permeability indices in the adult respiratory distress syndrome. *Am Rev Respir Dis* **1986**;133:1001-1005
  39. Mason GR, Duane GB, Mena I, Effros RM. Accelerated solute clearance in *Pneumocystis carinii* pneumonia. *Am Rev Respir Dis* **1987**;135:864-868
  40. Barrowcliffe MP, Otto C, Jones JG. Pulmonary clearance of <sup>99m</sup>Tc-DTPA: influence of background activity. *J Appl Physiol* **1988**;64:1045-1049
  41. Gorin AP, Kohler J, Denardo G. Non-invasive measurement of pulmonary transvascular flux in normal man. *J Clin Invest* **1980**;66:869-877
  42. Dauber IM, Pluss WT, van Grondelle A, Trow RS, Weill JV. Specificity and sensitivity of non-invasive measurement of pulmonary vascular protein leak. *J Appl Physiol* **1985**;59:564-574
  43. Rocker GM, Pearson D, Stephens M, Shale DJ. An assessment of a double-isotope method for the detection of transferrin accumulation in the lungs of patients with widespread pulmonary infiltrates. *Clin Sci* **1988**;75:47-52
  44. Rocker GM, Morgan AG, Pearson D, Basran GS, Shale DJ. Pulmonary vascular permeability to transferrin in the pulmonary oedema of renal failure. *Thorax* **1987**;42:620-623
  45. Taplin GV, Chopra SK, MacDonald NS, Elam D. Imaging small pulmonary ischaemic lesions after radioactive carbon monoxide inhalation. *J Nucl Med* **1976**;17:866-871
  46. Ewan PW, Jones HA, Rhodes CG, Hughes JMB. Detection of intrapulmonary haemorrhage with carbon monoxide uptake: application in Goodpasture's syndrome. *N Engl J Med* **1976**;295:1391-1396
  47. Wiener CM, McKenna WJ, Myers MJ, Lavender JP, Hughes JMB. Left lung ventilation is reduced in patients with an enlarged heart in the supine but not in the prone position. *Am Rev Respir Dis* **1990**;141:150-155
  48. Rhodes CG, Valind SO, Brudin L, et al. Modulation of pulmonary glucose utilisation by dietary state in man. *Clin Sci* **1985**;68:21P
  49. Nolop KB, Rhodes CG, Brudin LH, et al. Glucose utilization in vivo by human pulmonary neoplasms. *Cancer* **1987**;60:2682-2689
  50. Pantin CF, Valind SO, Sweatman M, et al. Measures of the inflammatory response in cryptogenic fibrosing alveolitis. *Am Rev Respir Dis* **1988**;138:1234-1241
  51. Hughes JMB, Rhodes CG, Brudin LH, Valind SO, Pantin C. Contribution of the positron camera to studies of regional lung structure and function. *Eur J Nucl Med* **1987**;13:537-541
  52. Haslett C, Clark RJ, Jones HA, Krausz T, Rhodes CG. Neutrophil metabolic activity in localised pulmonary inflammation measured noninvasively by positron emission tomography (PET). *Physiologist* **1989**;32:210
  53. Swenson ER, Rhodes CG, Araujo L, et al. Intrathoracic localisation and quantitation of tissue carbonic anhydrase in dogs studied with PET. *Physiologist* **1989**;32:210
  54. Farde L, Hall H, Ehrin E, Sedvall G. Quantitative analysis of D2 dopamine receptor binding in the living human brain by PET. *Science* **1986**;231:258-261
  55. Syrota A, Comar D, Pailotin G, et al. Muscarinic cholinergic receptor in the human heart evidenced under physiological conditions by positron emission tomography. *Proc Natl Acad Sci USA* **1985**;82:584-588